Bioactive Materials 20 (2023) 81–92

Contents lists available at ScienceDirect

Bioactive Materials

journal homepage: www.keaipublishing.com/en/journals/bioactive-materials

Electrical charge on ferroelectric nanocomposite membranes enhances SHED neural differentiation

Xiaochan Li [a,b,c,1], Boon Chin Heng [d,1], Yunyang Bai [a], Qianqian Wang [a], Min Gao [a], Ying He [a], Xinwen Zhang [e,***], Xuliang Deng [a,f,**], Xuehui Zhang [b,f,*]

[a] Department of Geriatric Dentistry, Peking University School and Hospital of Stomatology, Beijing, 100081, PR China
[b] Department of Dental Materials & Dental Medical Devices Testing Center, Peking University School and Hospital of Stomatology, Beijing, 100081, PR China
[c] Department of Prosthodontics, Peking University School and Hospital of Stomatology, Beijing, 100081, PR China
[d] Central Laboratory, Peking University School and Hospital of Stomatology, Beijing, 100081, PR China
[e] Center of Implant Dentistry, School and Hospital of Stomatology, China Medical University, Liaoning Provincial Key Laboratory of Oral Diseases, Shenyang, 110002, PR China
[f] National Engineering Research Center of Oral Biomaterials and Digital Medical Devices, NMPA Key Laboratory for Dental Materials, Beijing Laboratory of Biomedical Materials, Peking University School and Hospital of Stomatology, Beijing, 100081, PR China

ARTICLE INFO

Keywords:
Surface charge
Electric polarization
Dose-response effect
Electrical microenvironment
Neurogenesis

ABSTRACT

Stem cells from human exfoliated deciduous teeth (SHED) uniquely exhibit high proliferative and neurogenic potential. Charged biomaterials have been demonstrated to promote neural differentiation of stem cells, but the dose-response effect of electrical stimuli from these materials on neural differentiation of SHED remains to be elucidated. Here, by utilizing different annealing temperatures prior to corona poling treatment, $BaTiO_3$/P(VDF-TrFE) ferroelectric nanocomposite membranes with varying charge polarization intensity ($d_{33} \approx 0$, 4, 12 and 19 pC N^{-1}) were fabricated. Enhanced expression of neural markers, increased cell elongation and more prominent neurite outgrowths were observed with increasing surface charge of the nanocomposite membrane indicating a dose-response effect of surface electrical charge on SHED neural differentiation. Further investigations of the underlying molecular mechanisms revealed that intracellular calcium influx, focal adhesion formation, FAK-ERK mechanosensing pathway and neurogenic-related ErbB signaling pathway were implicated in the enhancement of SHED neural differentiation by surface electrical charge. Hence, this study confirms the dose-response effect of biomaterial surface charge on SHED neural differentiation and provides preliminary insights into the molecular mechanisms and signaling pathways involved.

1. Introduction

Stem cell transplantation therapy for repairing central nervous system defects, including brain and spinal cord injuries, faces several major challenges in clinical translation [1]. As mature neurons lack regenerative capacity upon damage or injury [2], finding an adequate stem cell source and developing better techniques to induce stem cell differentiation into functional neural lineages, have always been the primary focus of neural tissue engineering [3,4]. Cellular electrical activity is well-known to play key roles in the early development of the central and peripheral nervous systems [5], regulating the differentiation, migration and spatial organization of neural stem/progenitor cells [6,7]. Hence, a biomimetic strategy through the use of electroactive biomaterials to provide a conducive pro-neurogenic electrical microenvironment for inducing and promoting adult stem cell neural differentiation has attracted much attention in recent years [8–10]. Nevertheless, most electroactive materials require an external energy input and wire connection, which increases the risk of surgical complications,

Peer review under responsibility of KeAi Communications Co., Ltd.
* Corresponding author. Department of Dental Materials & Dental Medical Devices Testing Center, Peking University School and Hospital of Stomatology, Beijing, 100081, PR China.
** Corresponding author. Department of Geriatric Dentistry, Peking University School and Hospital of Stomatology, Beijing, 100081, PR China.
*** Corresponding author.
E-mail addresses: zhangxinwen@cmu.edu.cn (X. Zhang), kqdengxuliang@bjmu.edu.cn (X. Deng), zhangxuehui@bjmu.edu.cn (X. Zhang).
[1] These authors contributed equally to this work.

https://doi.org/10.1016/j.bioactmat.2022.05.007
Received 8 February 2022; Received in revised form 4 May 2022; Accepted 5 May 2022

particularly pathogenic infection after implantation [11]. Alternatively, self-powered triboelectric or piezoelectric scaffolds to induce neurogenic differentiation of mesenchymal stem cells, have attracted more attention for tissue engineering applications recently [12]. Nevertheless, these still require either wires to connect implanted electrodes or external mechanical force loading. Alternatively, biomaterials that could realize electrodeless and self-charging functions would be particularly promising for tissue engineering applications.

Ferroelectric materials are self-charged after treatment with an external electric field because of their spontaneous polarization properties, which can be considered as remanent polarization [13]. The surface charge intensity derived from the electrical polarization can be precisely controlled by adjusting polarization parameters and material composition ratios. Moreover, the surface electrical polarization of ferroelectric materials often exhibits long-term stability, which could provide stable culture substrata for inducing lineage-specific differentiation of adult stem cells [14]. More recently, we together with another group have fabricated self-charged P(VDF-TrFE)-based ferroelectric composite materials with controllable surface intensity to induce lineage-specific differentiation of mesenchymal stem cells [15–17]. Nevertheless, the dose-response effect of self-charged ferroelectric materials in inducing stem cell neurogenesis is still unclear.

Most previous studies have utilized either growth factors or chemical inducers to induce neural differentiation of dental stem cells, such as stem cells from human exfoliated deciduous teeth (SHED) or dental pulp stem cells (DPSC) [18]. However, the effectiveness of electroactive materials in inducing neural differentiation of dental stem cells and the underlying biological mechanisms involved have not yet been rigorously characterized. Hence, this study utilized ferroelectric nanocomposite membrane including P(VDF-TrFE) matrix and $BaTiO_3$ nanoparticles (BTO-NPs) fillings as charged material models. By adjusting the annealing pretreatment temperature, combined with corona polarization treatment, the surface charge intensity of the ferroelectric nanocomposite membrane can be precisely controlled. Then the dose-response effects of surface charge of the nanocomposites on SHED neural differentiation were investigated (Schematic Fig. 1). Additionally, the possible underlying molecular mechanisms including mechanosensing and its associated signal transduction (mechanotransduction), as well as intracellular calcium activation were explored.

2. Materials and methods

2.1. Fabrication and differential polarization of $BaTiO_3$/P(VDF-TrFE) nanocomposite membranes

The $BaTiO_3$/P(VDF-TrFE) nanocomposite membranes were fabricated based on our previously reported protocol [16]. Briefly, BTO NPs (99.9%, average particle size of 100 nm, Alfa Aesar) were dispersed ultrasonically in 0.01 mol/L of dopamine hydrochloride (99%, Alfa Aesar) aqueous solution, followed by stirring for more than 12 h at 60 °C to modify the nanoparticles. Subsequently, the modified BTO NPs together with the P(VDF-TrFE) co-polymer powders (70/30 mol% VDF/TrFE, Arkema) were both dissolved in N, *N*-dimethylformamide (DMF). After at least 3 rounds of repeated stirring and ultrasonication, the stable suspension was then cast into membranes of approximately 30 μm thickness and then dried at 55 °C for 10 h for solvent volatilization. For surface charge polarization, the membranes were annealed at 90 °C and 120 °C respectively for 30 min and were then treated by corona poling at room temperature for 30 min. Therefore, the membranes were differentially polarized with varying surface charges, with non-charged (NC, 55 °C, no poling), low-charged (LC, 55 °C, poling), mid-charged (MC, 90 °C annealing, poling) and high-charged (HC, 120 °C annealing, poling) nanocomposite membranes being obtained.

2.2. Characterization of $BaTiO_3$/P(VDF-TrFE) nanocomposite membranes

The surface morphology of the BTO/P(VDF-TrFE) composite membranes after annealing and polarization were examined by field emission scanning electron microscopy (FE-SEM, S-4800, HITACHI). The surface roughness of the membranes was characterized by atomic force microscopy (AFM, Bruker), while the surface wettability of the membranes was evaluated by water contact angle measurements, which were carried out on a video contact angle instrument (JC2000C1, Shanghai Glory Numeral Technique and Device Co., Ltd.). The Young's modulus and tensile strength were evaluated using the universal mechanical machine (INSTRON-1121) according to GB13022-91.

For ferroelectric property characterization of the membranes before corona poling, the polarization-electric field (P-E) loop was analyzed using a commercial ferroelectric analyzer (TF1000, aixACCT System GmbH). The piezoelectric coefficient (d_{33}) was detected by a piezoelectric coefficient meter (ZJ-3AN, IACAS), while the surface electrical potential was measured by Scanning Kelvin Probe Microscopy (SKPM) (Multimode 8, Bruker).

2.3. Cell culture

Stem cells from human exfoliated deciduous teeth (SHED) were provided by ORAL STEM CELL BANK run by Beijing Tason Biotech Co., Ltd. (http://www.kqgxbk.com). The culture media used in this study was as follows: (i) Normal culture medium composed of high-glucose DMEM supplemented with 10% (v/v) FBS and 1% (v/v) penicillin-streptomycin solution. (ii) Neural induction medium (NI), as reported in our previous study [19], which was composed of a mixture of DMEM/F12 and Neurobasal media [1:1 v/v] supplemented with 0.5% (v/v) N2, 1% (v/v) B27, 100 mM cAMP, and 20 ng/mL bFGF.

2.4. qRT-PCR analysis

A RNeasy Plus Mini kit (Qiagen) was used to extract and purify cellular RNA. Reverse transcription was achieved with PrimeScript™ RT reagent Kit (TaKaRa). The SYBR Premix Kit (TaKaRa) and PCR thermal cycler (TaKaRa) were used for qPCR. The cycle threshold (CT) value of the sample was normalized to the value of the GAPDH housekeeping gene, and the relative expression was calculated using the $2^{-\triangle\triangle CT}$ method. The primer sequences are shown in Table S1.

2.5. Immunocytochemistry

SHED were cultured on composite membranes within 6-well plates for 2d and 8d, respectively, in designated culture media. After *in vitro* culture at 37 °C within a humidified atmosphere of 5% CO_2 at scheduled time points, the cells were washed with 1 × PBS, fixed with 4% (w/v) paraformaldehyde (pH 7.4) for 15 min at room temperature and then rinsed in PBS three times. After permeabilization with 0.1% (w/v) Triton X-100 for 10 min, the cells were blocked with 5% (v/v) bovine serum albumin (BSA, Sigma; diluted with PBS) for 1 h. The samples were then incubated with the following primary antibodies specific for either MSI1 (ab52865, Abcam) or TUBB3 (ab18207, Abcam) overnight at 4 °C. After thorough rinsing, the samples were incubated with the secondary antibody goat anti-rabbit IgG H&L Alexa Fluor 488 (ab150077, Abcam) for 1 h. DAPI (D9542; Sigma-Aldrich) and Rhodamine Phalloidin (RM02835; Abclonal) were used to stain the cell nuclei and cytoskeleton, respectively. Then, the cells were observed under a laser confocal microscope (Leica, TCS-SP8 DIVE). Leica LAS software was used to detect and analyze fluorescence intensity. Image J was used to calculate cell spreading area and aspect ratio. All measurements were performed using a minimum sample size of 50 cells in each group. Image J software was used to track neurite outgrowths from the differentiating SHED, and the length from the neuronal somata to axon terminal was calculated

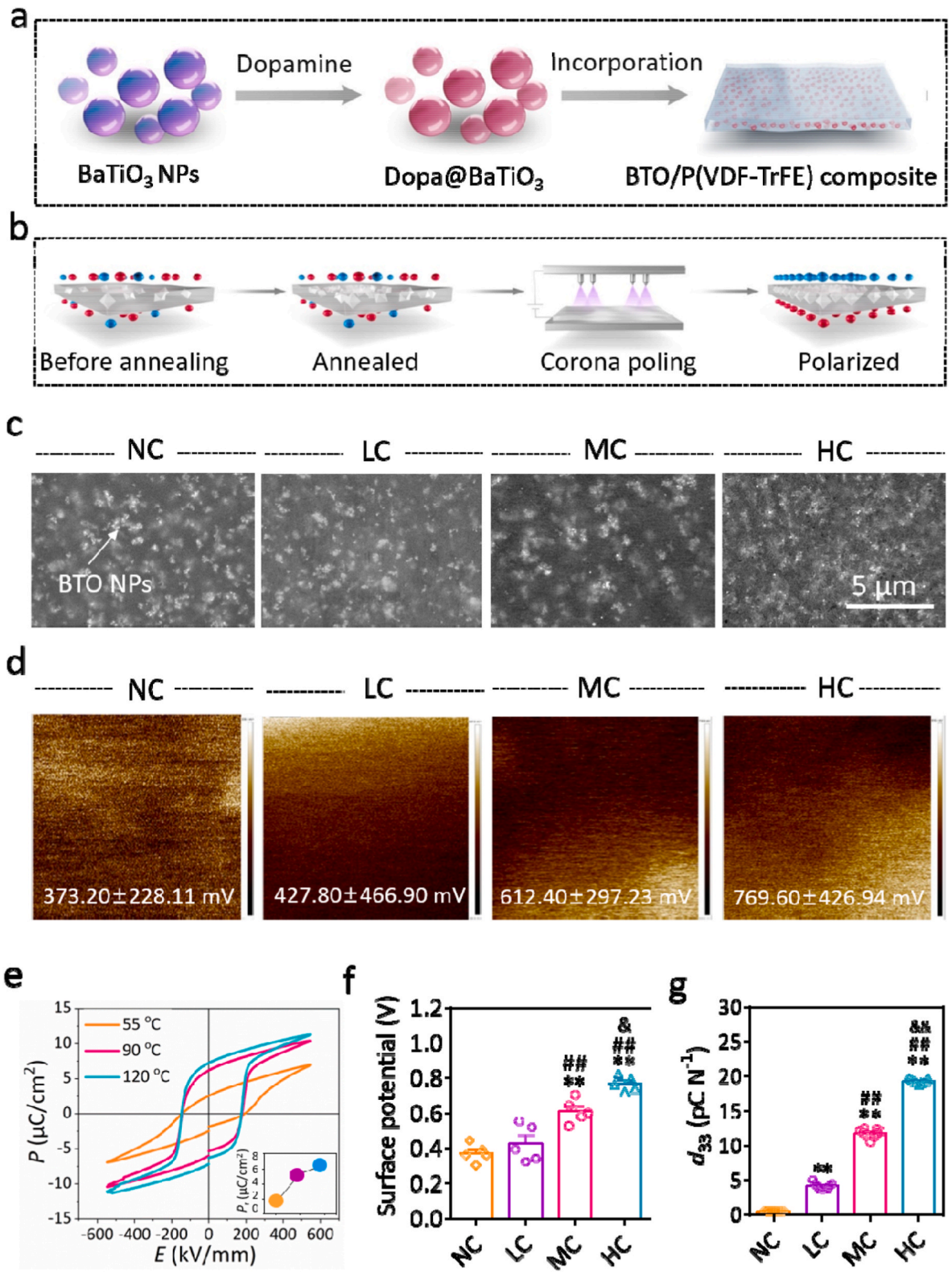

Fig. 1. Fabrication and characterization of BTO/P(VDF-TrFE) nanocomposite membranes with different surface electrical polarization intensity. (a) Fabrication process of BTO/P(VDF-TrFE) nanocomposite membrane. (b) Annealing followed by subsequent corona poling of nanocomposites. (c) Representative SEM images of nanocomposite membranes with different surface charge dose. The white arrow denotes the BTO NPs. (d) Relative surface potential of nanocomposite membranes with different surface charge dose. (e) Hysteresis loop of BTO/P(VDF-TrFE) nanocomposite membranes with different annealing temperatures. The inset is the residual polarization intensity (Pr). (f) Quantitative statistical analysis of surface potential of the differentially charged nanocomposite membranes (n = 5). (g) The piezoelectric constant d_{33} values of the differentially charged nanocomposite membranes (n = 5). *: compared with NC; #: compared with LC; &: compared with MC. ($^{**}p < 0.01$, $^{\#\#}p < 0.01$, $^{\&}p < 0.05$, $^{\&\&}p < 0.01$).

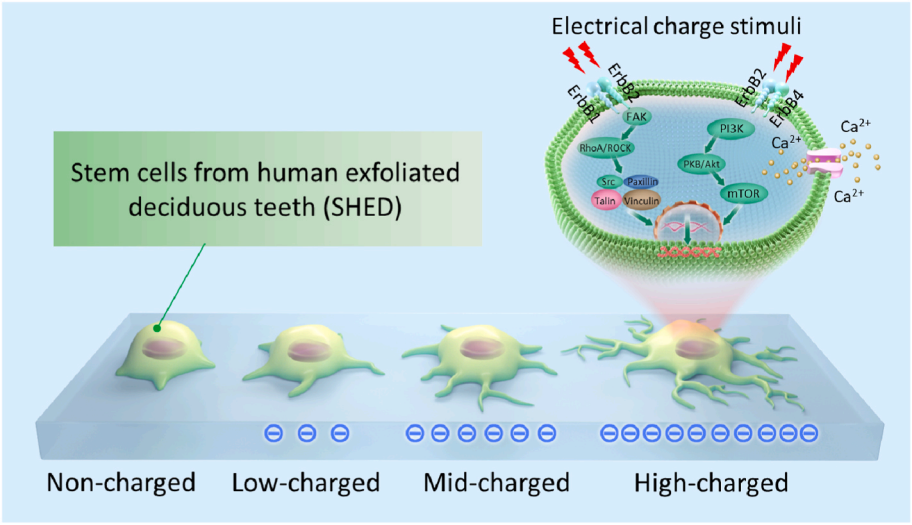

Schematic Fig. 1. Illustration of how regulating surface electrical polarization intensity on ferroelectric nanocomposite membranes can enhance SHED neurogenic differentiation. The neurogenic differentiation of SHED appears to be dose-dependently affected by surface charge, accompanied by changes in cell morphology, including increased cell spreading area and enhanced neurite length. Further molecular mechanism analysis revealed that surface charge stimulates opening of calcium channels on the cell membrane, resulting in increase in the intracellular calcium concentration, which might lead to activation of pro-neurogenic signaling pathways in SHED including the ErbB signaling pathway, cell focal adhesion-related pathways and regulation of actin cytoskeleton. On one hand, ErbB-1/2 acts on FAK and downstream Src, triggering the mechanosensing pathway RhoA/Rock, increasing Paxillin phosphorylation, which in turn might facilitate neurite outgrowths. On the other hand, the PI3K/Akt/mTOB signaling pathway is also triggered by ErbB-2/4.

and recorded as neurite length. More than 30 neurite outgrowths in each group were tracked and statistically analyzed.

2.6. Western blot analysis

Cells were lysed with RIPA buffer (R0010, Solarbio) containing 1% protease inhibitor (ab65621, Abcam) on ice to extract total cell protein. The samples were denatured with a 1/5 volume of SDS-PAGE sample buffer(6 ×) (P0015F, Beyotime) at 100 °C for 5 min to acquire the final protein sample. Then the protein samples were subjected to electrophoresis on a 10% (w/v) SDS-PAGE gels. After transferring to a PVDF membrane, this was washed by 1 × TBST buffer (T1081, Solarbio) and then blocked with TBST buffer containing 5% (w/v) milk powder (1706404, Bio-Rad) for 1 h. This was followed by incubation overnight at 4 °C individually with the following primary antibodies specific for: GAPDH (ab8245, Abcam), MSI1 (ab52865, Abcam), TUBB3 (ab18207, Abcam), FAK (PTK2) (ab40794, Abcam), Paxillin (ab32084, Abcam) and p-Paxillin (ab109547, Abcam). Next, the membranes were washed with TBST for 3 times, and were incubated with the following secondary antibodies including HRP goat anti-rabbit IgG(H + L) (A0208, Beyotime, China) and HRP goat anti-mouse IgG(H + L) (A0216, Beyotime) for 1 h. The Immobilon Western (WBKLS0100, Millipore) kit was used to visualize immune complexes, and the protein expression levels were analyzed with the ChemiDoc™ Touch Imaging System (17024024, Bio-Rad). The Western Blots of each target protein was replicated three times. The gray value was normalized with GAPDH, and the relative expression of the control group NC was set to an arbitrary value of 1.0 for standardization and further comparison between groups.

2.7. Flow cytometry analysis

Intracellular calcium concentration was analyzed by flow cytometry. SHED was cultured on BTO membranes separately for 2d and 8d. Then the cells were treated with normal culture medium supplemented with Fluo-4 AM fluorescent probe (HY-101896, MCE) for 30 min. After washing with 1 × PBS, the cells were enzymatically dissociated, collected, centrifuged and then resuspended in 1 × PBS within flow cytometry tubes. This was followed by flow cytometry analysis with Calibur1 (20042466, Bio-Rad), at a fluorescence emission wavelength of 516 nm.

2.8. RNA sequencing

SHED were seeded on the NC and HC- nanocomposite membranes in normal culture medium for 24 h, and then the medium was changed to neural induction medium for another 8d. TRIzol (15596026, Invitrogen) was used to collect cell lysates. Five independent replicate samples from every group were sent to Beijing Cnkingbio Biotechnology Co., Ltd. for the global transcriptome analysis. Before transcriptome sequencing, the samples were subjected to quality-control inspection. All samples met the following requirements: (i) RNA concentration >50ng/ul, total amount >1.5 μg; (ii) the 260nm/280 nm absorbance ratio was nearly within the range of 1.8–2.1, and the sample was free of macromolecular pollution; (3) the sample remains intact without degradation. The KEGG enrichment analysis of differentially-expressed genes was performed. KEGG is a database and resource for the public to understand the advanced functions of biological systems. Differentially-expressed genes were significantly enriched for KEGG pathways with a p value less than 0.05 (adjusted p values were used to screen different candidate genes). In the differential expression analysis, $p < 0.05$ and $|\text{FoldChange}| \geq 1.5$ were set as the statistical thresholds for significantly different expression. Finally, the signaling pathways were enriched and differentially expressed genes identified by RNA-Seq were further verified by qRT-PCR.

2.9. Statistical analysis

Results were presented as mean ± SEM. All experiments were performed in triplicates. Statistical analysis between more than two groups was performed by one-way unstacked ANOVA and post-hoc Tukey HSD testing. Statistical analysis between two groups was performed by independent sample t-tests. The data was classified by the values of p and denoted by (*) for $p < 0.05$, or (**) for $p < 0.01$. (*/**: compare with NC, #/##: compare with LC, &/&&: compare with MC).

3. Results and discussion

3.1. Regulation of surface charge intensity of ferroelectric nanocomposite membranes

In order to achieve varying surface charge intensities on the ferroelectric nanocomposite membrane, we utilized a strategy of controlling the annealing temperature combined with corona poling treatment of the BTO/P(VDF-TrFE) nanocomposite membrane. Firstly, the surface of BTO-NPs was modified with dopamine and then incorporated into P(VDF-TrFE) matrix to form a nanocomposite membrane (Fig. 1a) as described in our previous study [16]. Then the membrane samples were subjected to annealing treatments at different temperatures (90 °C and

120 °C) (Fig. 1b). As compared with the membrane without annealing treatment (Drying at 55 °C), the remanent polarization of the nanocomposite membrane could be significantly improved after annealing treatment at both 90 °C and 120 °C (Fig. 1e). In particular, the nanocomposite membrane annealed at 120 °C maintains a higher remanent polarization, and is considered to reach the curie temperature of P (VDF-TrFE) [20]. In previous studies [15], it was confirmed that continuing to increase the annealing temperature would lead to cracks on the material surface, as well as increasing brittleness of the solid material, limiting its clinical applications. Previous studies have confirmed that annealing at the Curie temperature can significantly increase the ferroelectric β-phase content of P(VDF-TrFE) [21]. Therefore, in this study, we achieved controllable remanent polarization by adjusting the annealing temperature, which enables differential polarization of surface charge parameters of the nanocomposite membrane.

We further carried out corona poling of the nanocomposite membranes to achieve surface charge polarization. Firstly, the relative surface potential of nanocomposite membranes was characterized by scanning Kelvin probe microscopy (SKPM) (Fig. 1d). As expected, corona poling treatment significantly increased the relative surface potential (referred to as LC) of the unannealed membrane, as compared with the untreated membrane (referred to as NC). The relative surface potential of the 90 °C annealed membrane is significantly higher than that of the unannealed group after corona polarization treatment under the same conditions, which is referred to as MC. Apparently, the 120 °C annealed membrane exhibited the highest surface potential after the same corona poling treatment (referred to as HC). The quantitative analysis of the relative surface potential also verified this trend (Fig. 1f). The different surface charge parameters on the nanocomposite membranes were further confirmed by measuring the piezoelectric coefficient (d_{33}) (Fig. 1g). The d_{33} of the annealed membrane was significantly higher than that of the unannealed membrane ($d_{33} \approx 4$ pC N^{-1}), and furthermore, the average d_{33} value of the 120 °C annealed membrane ($d_{33} \approx 19$ pC N^{-1}) was significantly higher than the 90 °C annealed membrane ($d_{33} \approx 12$ pC N^{-1}). As reported in a previous study, the difference in surface charge imparted by corona poling treatment of the nanocomposite membranes with different annealing pretreatments is mainly due to annealing pretreatment increasing the β-phase content of P(VDF-TrFE); with incorporation of nanoscale ferroelectric BTO particles increasing its interface electrical polarization with the P(VDF-TrFE) matrix [16]. Furthermore, the charge polarization homogeneity of the membrane surface was investigated by examining the d_{33} distribution. From the contour map (Fig. S3), it could be observed that the surface electrical charge was distributed uniformly on the membrane surface for all groups. This suggests that membrane surface charges can provide homogeneous electrical stimuli to cellular responses. These results thus indicate that varying the annealing temperature combined with corona poling technique, could be a practical method for achieving differential regulation of surface charge parameters of nanocomposite membranes.

The other surface properties of the nanocomposite membranes were investigated to exclude artefactual interference from differences in physical surface properties. It was found that the BTO NPs fillers are uniformly dispersed within the P(VDF-TrFE) matrix (Fig. 1c), and there is no obvious difference in the surface structure between nanocomposite membranes with different charge parameters, as observed under a high-magnification field of view (Fig. S1). This indicates that annealing treatment below 120 °C and subsequent corona poling had no effect on the surface morphology of the material, with no significant difference in surface roughness (Figs. S2a and b) and surface wettability (Fig. S2c), except for tensile strength (Fig. S4a) and elastic modulus (Fig. S4b) increasing with annealing temperature. According to our study, as well as other previous studies, the tensile strength and elastic modulus changes at this magnitude will not affect the biological functions of stem cells [15,16]. This thus enabled us to focus exclusively on the effects of surface charge intensity on the biological properties of the nanocomposite membranes, excluding artefactual interference from other general physico-chemical properties.

3.2. Surface electrical charge promotes earlier neural differentiation of SHED in a dose-dependent manner

To evaluate whether surface electrical charge on the ferroelectric nanocomposite membranes can enhance neurogenic differentiation of SHED, these cells were initially cultured on the nanocomposite membranes with different charge polarization parameters for 2 days in neural induction medium based on our preliminary experiment, in which we found that the neural induction of SHED was not obvious at timepoints earlier than 2 days, such as 6 h, 12 h and 1d (data not shown). Subsequently, the cells were subjected to immunostaining for detection of the earlier neurogenic marker, Musashi1 (MSI1), which is widely-regarded to be the canonical marker of neural stem cells and progenitor cells [22]. It is a transcription inhibitor that can directly regulate the expression of target proteins numb and p21 (CIP-1), which are mainly found in neural stem cells [23]. MSI1 is therefore an appropriate marker of early neurogenesis. Because Musashi1 is a transcription factor, immunofluorescence staining is predominantly localized in the cell nuclei (Fig. 2a). As shown in Fig. 2a, the immunocytochemical staining results showed a gradual increase in MSI1 expression by SHED, with increasing surface charge on the nanocomposite membrane, which clearly demonstrates that surface charge enhances earlier neurogenic differentiation of SHED in a dose-dependent manner. This was corroborated by quantification of immunofluorescence staining intensities (Fig. 2b). It was found that the fluorescence intensity of the LC, MC and HC groups were significantly increased compared with the NC group, with the HC group exhibiting the highest value (Fig. 2b). In addition, obvious differences in cell morphology can be observed between the differentially charged nanocomposite membranes. In particular, within the HC group, the cells exhibited a larger spreading area and more elongated cell morphology (Fig. 2a, Fig. S6). Interestingly, there was also observed to be a concomitant gradual increase in F-actin expression by SHED, with increasing surface charge of the nanocomposite membrane (Fig. 2a). This may be related to increased cell spreading area (Fig. S5a), cell elongation (Fig. S5b) and increased neurite outgrowth (Fig. 2c), with increasing surface charge of the nanocomposite membranes. F-actin is a major component of the cytoskeleton, which is known to play a key role in neurite outgrowths and axonal formation during neurogenesis [23,24].

The qRT-PCR analysis showed that both early neural markers MSI1 and Nestin displayed a trend towards increased expression, with increasing surface charge of the nanocomposite membrane (Fig. 2d). Additionally, Western blots also detected a trend towards increased protein expression levels of MSI1 being induced by increasing surface charge on the nanocomposite membrane, after 2d of neural induction culture (Fig. 2e and f). These markers are associated with neuronal cytoskeleton formation [25–27], which was also confirmed by the immunocytochemical staining results (Fig. 2a). Interestingly, the expression of mid-to-later stage neural markers Neuron specific enolase (ENO2) and Neurofilament medium (NEFM) were significantly higher in the HC group than in the other groups (Fig. 2d), suggesting that increased surface charge might hasten neurogenic differentiation of SHED. Hence, the dose-response effect of increasing surface charge on hastening neural differentiation of SHED was demonstrated.

The activation of transmembrane calcium channels and intracellular calcium transients play an important role in regulating the neurogenic differentiation of stem cells [28,29]. Hence, in order to explore the underlying mechanisms of the dose-response effect of surface charge on SHED neural differentiation, we investigated how the nanocomposite membranes affect the intracellular calcium concentration in SHED. After neural induction culture for 2d, it was observed that with increasing surface charge, the calcium fluorescence intensity histogram shifted to the right (Fig. 2g), thus indicating that the intracellular calcium concentration gradually increased from the NC to HC groups. The statistical

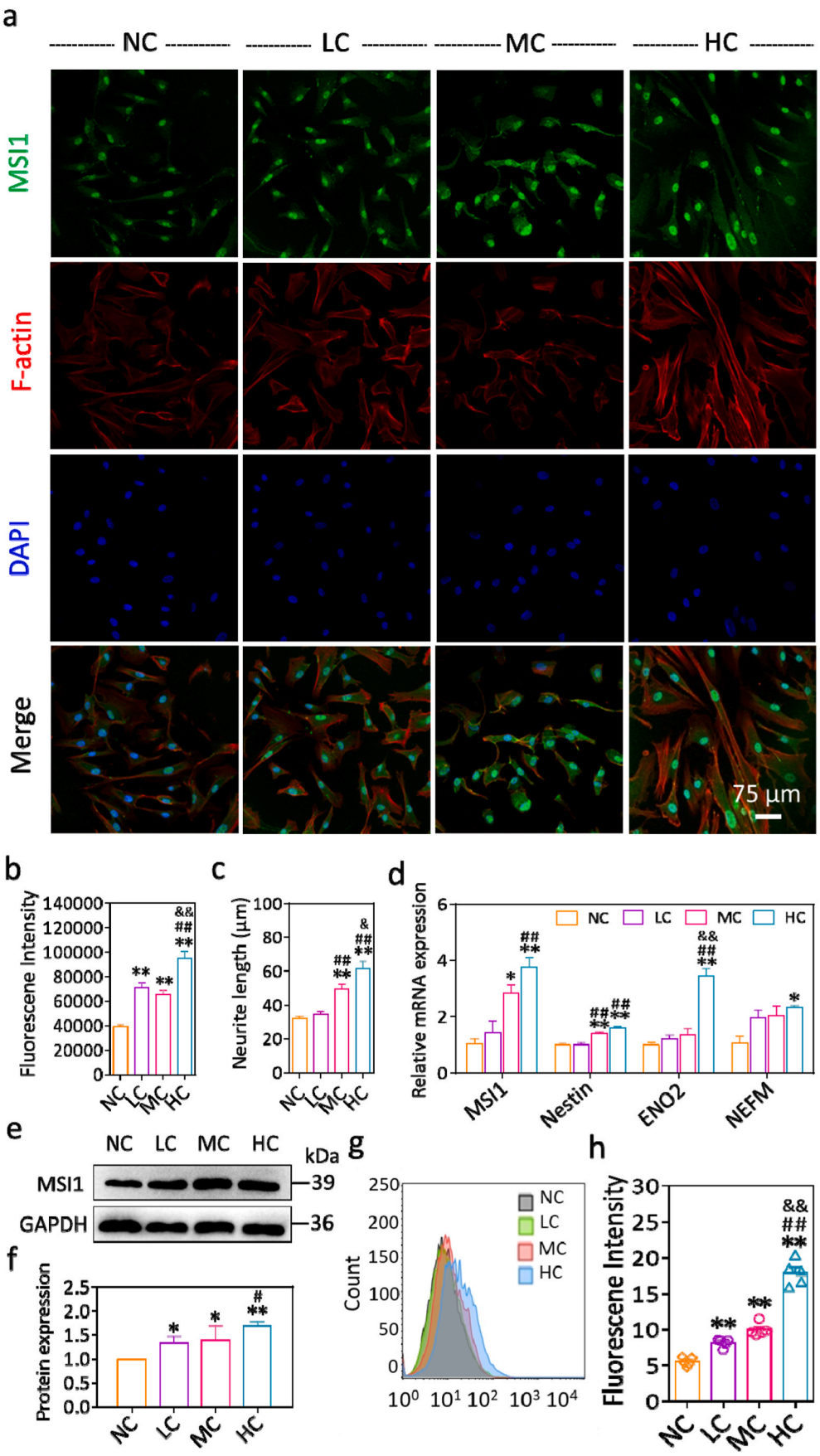

Fig. 2. Dose-response effect of surface charge of nanocomposite membranes on earlier stage neural differentiation of SHED. (a) Immunocytochemical staining for detection of MSI1 (Green), F-actin (red) and nuclear DNA (DAPI, blue) in SHED cultured on nanocomposite membranes with varying surface charges in neural induction medium for 2 days. With increasing surface charge of the polarized BTO membranes, the expression of early neural marker MSI1 increased significantly, and showed obvious nuclear localization. (Scale bar: 75 μm) (b) Immunofluorescence staining intensities of MSI1 expression in SHED cultured in neural induction medium for 2 days (n = 50). (c) The average neurite length of neuron-like cells induced by nanocomposite membranes in neural induction medium for 2 days (n = 35). (d) mRNA expression levels of neurogenic markers in SHED cultured in neural induction medium for 2 days. (e) Protein expression levels of neurogenic markers MSI1 in SHED after culture in neural induction medium for 2 days. (f) Quantitative analysis of protein expression levels after culture in neural induction medium for 2 days (n = 3). (g) Flow cytometry analysis of intracellular calcium ion concentration in SHED cultured on nanocomposite membranes for 2 days. (h) The fluorescence intensity of intracellular calcium in SHED cultured on nanocomposite membranes for 2 days.*: compared with NC; #: compared with LC; &: compared with MC. ($^{*}p < 0.05$, $^{**}p < 0.01$, $^{\#\#}p < 0.01$, $^{\&}p < 0.05$, $^{\&\&}p < 0.01$).

analysis of fluorescence intensity confirmed that the intracellular calcium concentrations of the LC, MC and HC groups were significantly higher than that of NC group, with the HC group displaying the highest value (Fig. 2h). High intracellular calcium concentration indicates that cells are in a highly active electrophysiological state, which is beneficial for triggering neurotransmitter release and regulating short-term neural plasticity [29].

3.3. Surface electrical charge enhances later neural differentiation of SHED in a dose-dependent manner

The normal functioning and electrical conductivity of neural tissues depend on neuronal maturation and axonal formation [30]. After confirming that earlier neurogenic differentiation of SHED can be enhanced by increasing surface charge after 2d of neural induction culture, we further investigated the effects of surface charge on the later neurogenic differentiation of SHED after 8d of neural induction culture.

Immunocytochemistry was carried out for detection of Beta III Tubulin (TUBB3) (Fig. 3a), which is involved in neurogenic differentiation of adult stem cells and is crucial for neuronal development and function [31]. It is involved in specific differentiation of the neuronal cell lineage and plays a key role in neuronal development and function [32]. Immunohistochemical studies reported that TUBB3 is widely expressed in immature neuronal cell bodies, dendrites, axons and axon terminals. TUBB3 is therefore a suitable marker for characterizing more mature neuronal cells, and its detection through immunostaining is useful for showing the typical morphology of dendrites and axons of neural lineage cells. TUBB3 staining is distributed throughout the entire cell spreading area, as would be expected of a cytosolic protein (Fig. 3a). After 8 days of neural induction culture, the immunostaining results showed that SHED displayed increasing expression of TUBB3, together with greater cell spreading area and cell elongation (Fig. 3a), with increasing surface charge of the nanocomposite membranes (Fig. 3a). The immunocytochemistry data was corroborated by quantitative analysis of fluorescence intensity of TUBB3 immunostaining, which showed a positive correlation between increase of fluorescence intensity with magnitude of surface charge (Fig. 3b). Similar to the 2 days timepoint data, it was again observed that there was larger spreading area and higher expression of F-actin within the charged groups versus uncharged NC group (Fig. 3a), which may be related to enhanced neurite outgrowth (Fig. 3c), increased cell spreading area (Fig. S5c) and greater cell elongation (Fig. S5d) with increasing surface charge.

These results were further validated by qRT-PCR analysis of neural marker expression at the mRNA level. The relative expression levels of later-stage neural markers [32,33] including TUBB3, ENO2, NCAM1 and NEFM displayed an increasing trend correlated to increasing surface charge on the nanocomposite membranes, with the HC group displaying the highest expression levels of all neural markers analyzed (Fig. 3d). Western blots confirmed increasing expression of TUBB3 at the protein level, with increasing surface charge of the nanocomposite membrane, during later neurogenic differentiation at the 8d timepoint (Fig. 3e and f). Hence, the 8d timepoint data again confirmed that electrical stimuli contributed significantly to enhancing SHED neural differentiation in an a dose-dependent manner.

After 8 days of neural induction, the intracellular calcium concentration of SHED was quantified again with flow cytometry. Similar to the 2d timepoint data, the fluorescence intensity histogram of each group at the 8d timepoint displayed an overall shift to the right, with an obvious dose-response relationship (Fig. 3g). Statistical analyses of the fluorescence intensity data confirmed this result, with the HC group exhibiting the highest value, which was nearly 4 times that of NC (Fig. 3h). The above results thus showed that the charged nanocomposite membranes promoted increase in the intracellular calcium concentration of SHED in a dose-dependent manner, triggering the signaling cascade reaction initiated by voltage-gated calcium channels, which in turn enhanced SHED neural differentiation in a dose-dependent manner.

3.4. Mechanotransduction signaling is implicated in enhancement of SHED neural differentiation by surface electrical charge

Based on the observed increased cell spreading area, greater cell elongation and enhanced neurite outgrowths with increasing surface charge (Figs. 2c and 3c and S5), it would be reasonable to hypothesize that the mechanosensing and mechanotransduction signaling axis is somehow involved in surface charge induced enhancement of SHED neurogenic differentiation. Indeed, the nervous system has long been known to be receptive to various biomechanical stimuli [34,35], which is closely related to nerve development and function.

Hence, in order to further explore the molecular mechanisms involved, we investigated the expression of focal adhesion kinase (FAK, also known as PTK2), and its downstream effectors Paxillin and p-Paxillin, which are known to play key roles in mechanosensing and mechanotransduction [36], as well as in regulating cell adhesion and spreading [37]. Moreover, the FAK-ERK signaling pathway is also known to play a crucial role in regulating stem cell differentiation fate [38]. The Western blot results showed that FAK and p-Paxillin were up-regulated while Paxillin was down-regulated with an increase of surface charge, both at the earlier timepoint of 2d (Fig. 4a) and later timepoint of 8d (Fig. 4b). This trend was further confirmed by the quantitative analysis of protein expressions (Fig. 4d & e). FAK acts as the molecular hub connecting integrin and downstream signaling molecules of the integrin signaling pathway [39]. Cytoskeletal proteins such as integrin, FAK and talin are co-localized and assembled together to form focal adhesion [40]. Paxillin is a cytoskeletal protein involved in actin-membrane attachment at the extracellular matrix site, which plays an important role in the integrin signaling transduction [41]. Integrin-mediated reorganization of the cytoskeleton requires the phosphorylation of Paxillin tyrosine residues [42]. As seen in Fig. 4a and b, there was a gradual increase in the expression of FAK and phosphorylated Paxillin (p-PXN) with increasing surface charge. The increased expression of p-PXN in turn upregulates the level of active Rac1 [43], thereby promoting the formation of cytoskeleton, which could explain why there is increased F-actin expression with increasing surface charge (Figs. 2a and 3a). Hence, these data thus indicate that the FAK mechanosensing signaling pathway is implicated in the dose-response effect of surface charge in enhancing SHED neural differentiation.

In order to further investigate in-depth the molecular events implicated in surface charge-induced enhancement of SHED neural differentiation, we conducted RNA-seq-based transcriptome profiling of SHED cultured on the high-charged nanocomposite membranes, after 8d of neural induction culture. From the heatmap, it can be observed that upon comparing with NC, neurogenic differentiation was increased, while osteogenic differentiation was inhibited on HC (Fig. 4c). This result was also confirmed by qPCR analysis of differentially expressed genes related to neurogenesis and osteogenesis in the RNA-Seq data (Fig. 4h). These findings clearly indicate that mechanotransduction plays an important role in the process by which electrical charge on the ferroelectric nanocomposite membranes enhances SHED neural differentiation. Not only because of increasing expression of FAK (PTK2) and p-Paxillin with increasing surface charge (Fig. 4a and b), but also because of the observed morphological changes (Figs. 2 and 3) and the RNA-Seq analysis data (Fig 4c, f-i). From the immunocytochemical staining images (Figs. 2a and 3a) and statistical analyses of neurite lengths (Figs. 2c and 3c), obvious morphological changes of cell outgrowths and extensions on the surface of the differentially-charged nanocomposite membranes can be observed. As widely reported in the scientific literature, cell adhesion, growth and functional differentiation on biomaterials are closely related to cell mechanotransduction, the formation of focal adhesions and cytoskeletal rearrangement. Additionally, KEGG enrichment analyses revealed the TOP10 enrichment pathways for functional annotation among the genes that were differentially-expressed, upon comparing the HC versus NC group at the

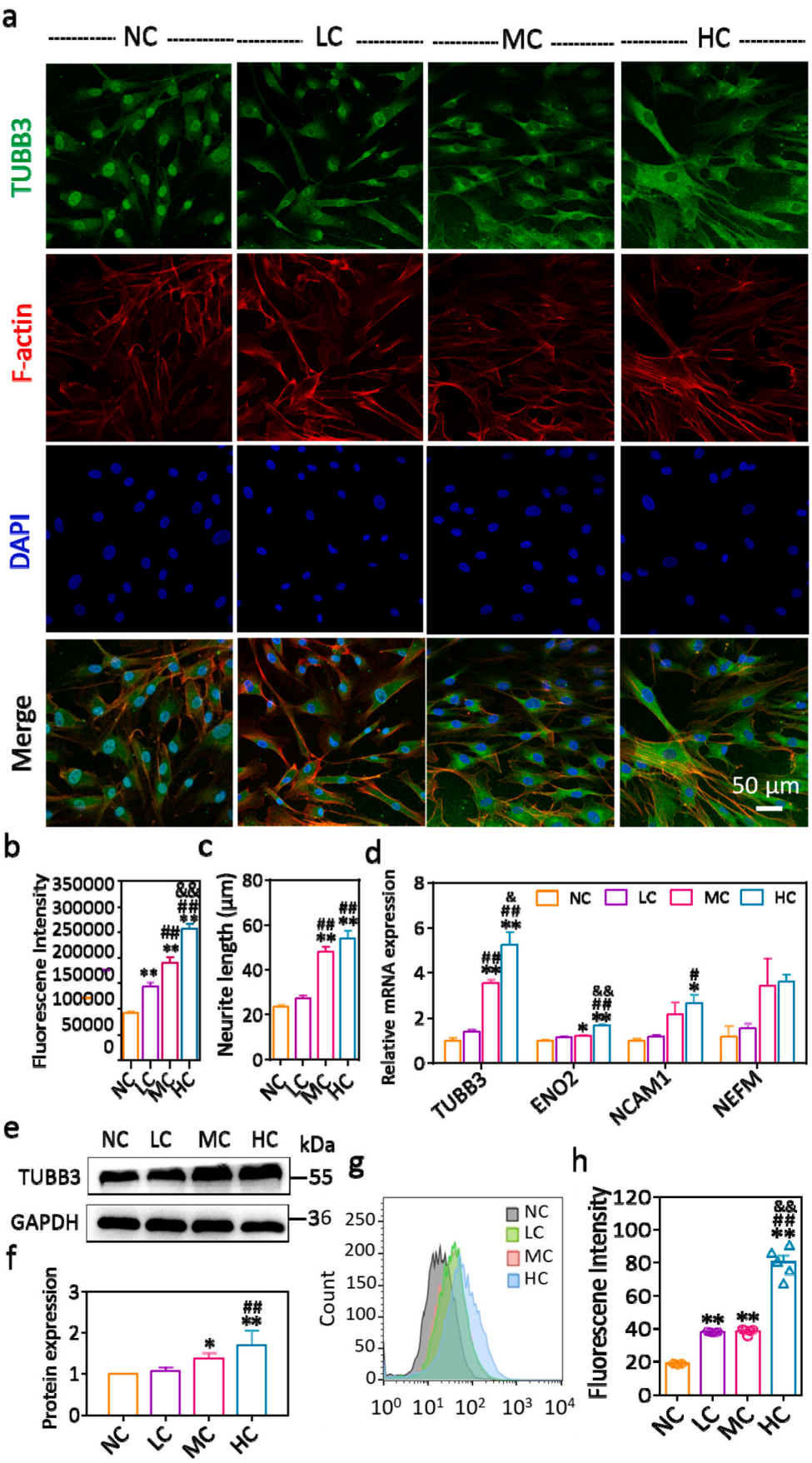

Fig. 3. Dose-response effect of surface charge of nanocomposite membranes on later stage neural differentiation of SHED. (a) Immunocytochemial staining for detection of TUBB3 (Green), F-actin (red) and nuclear DNA (DAPI, blue) in SHED cultured on nanocomposite membranes with varying surface charges for 8 days in neural induction medium. (Scale bar: 50 μm) (b) Immunofluorescence staining intensities of TUBB3 in SHED cultured in neural induction medium for 8 days (n = 50). (c) The average neurite length of neuron-like cells induced by nanocomposite membranes in neural induction medium for 8 days (n = 40). (d) mRNA expression levels of neurogenic markers in SHED cultured on nanocomposite membranes in neural induction medium for 8 days. (e) The protein expression levels of neurogenic markers TUBB3 in SHED with increasing surface charge of nanocomposite membranes, after culture in neural induction medium for 8 days. (f) Quantitative analysis of protein expression levels after culture in neural induction medium for 8 days (n = 3). (g) Flow cytometry analysis of intracellular calcium concentration in SHED cultured on nanocomposite membranes for 8 days. (h) The fluorescence intensity of intracellular calcium in SHED cultured on nanocomposite membranes for 8 days. *: compared with NC; #: compared with LC; &: compared with MC. ($^{*}p < 0.05$, $^{**}p < 0.01$, $^{\#}p < 0.05$, $^{\#\#}p < 0.01$, $^{\&}p < 0.05$, $^{\&\&}p < 0.01$).

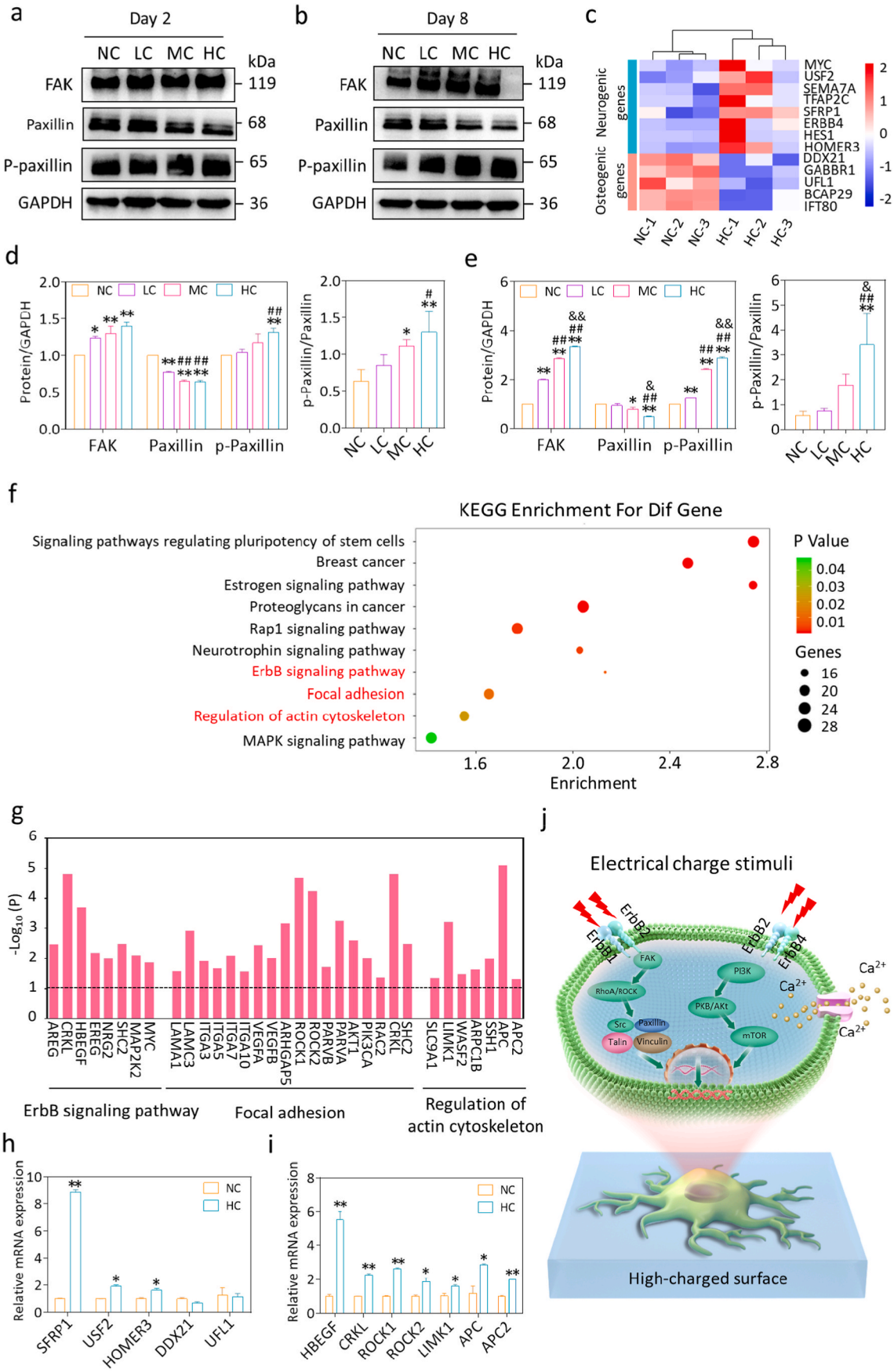

(caption on next page)

Fig. 4. Underlying molecular mechanisms and signaling pathways by which surface electrical charges on nanocomposite membranes enhance SHED neural differentiation. (a) Protein expression levels of the FAK (PTK2) mechanosensing pathway downstream effectors Paxillin and p-Paxillin in SHED cultured on nanocomposite membranes with varying surface charges in neural induction medium for 2 days. (b) Protein expression levels of Paxillin and p-Paxillin in SHED cultured on nanocomposite membranes with varying surface charge in neural induction medium for 8 days. (c) Heat map of up-regulated neurogenic promoting genes and down-regulated osteogenic-promoting genes in SHED on high-charged nanocomposite membranes after culture in neural induction medium for 8 days. (d) Quantitative analysis of protein expression levels of FAK, Paxillin, p-Paxillin and p-Paxillin/Paxillin in SHED after culture in neural induction medium for 2 days (n = 3). (e) Quantitative analysis of protein expression levels of FAK, Paxillin, p-Paxillin and p-Paxillin/Paxillin in SHED after culture in neural induction medium for 8 days (n = 3). (f) KEGG signaling pathway analysis of significantly differentially-expressed genes in SHED on high-charged nanocomposite membranes after culture in neural induction medium for 8 days. (g) The up-regulated gene expression of representative mechanosensing and neural differentiation signaling pathways enriched by KEGG analysis. (h) qPCR verification of differentially expressed genes related to neurogenesis and osteogenesis in the heat map of RNA-Seq analysis in Fig. 4c. (i) qPCR verification of differentially expressed genes of representative mechanosensing and neural differentiation signaling pathways enriched by KEGG analysis in Fig. 4g. (j) Schematic diagram of the possible underlying molecular mechanisms.

8d timepoint (Fig. 4f). In particular, the neurogenesis-related ErbB signaling pathway [44], cell focal adhesion-related pathways [45,46], and the regulation of actin cytoskeleton [47] were all found to be enriched (Fig. 4g). All these signaling pathways are related to mechanosensing and mechanotransduction. Hence our results provide strong evidence that cell adhesion and mechantransduction are closely associated with the enhancement of SHED neurogenic differentiation by surface charge on the nanocomposite membranes.

A schematic illustration of the signaling pathways and underlying molecular mechanisms by which SHED neural differentiation is enhanced by surface electrical charge is summarized in Fig. 4j. In response to electrical stimuli, activated ErbB-1/2 acts on FAK (PTK2) and downstream Src, involving self-phosphorylation of Tyr397 on FAK, which mediates the direct interaction between Src and FAK [48]. This in turn triggers the mechanosensing RhoA/Rock pathway, increasing Paxillin phosphorylation, as well as promoting cytoskeletal rearrangements and focal adhesion formation, which in turn might facilitate neurite outgrowths and promote cell elongation to form a more “neural-like” morphology. Fully-activated FAK can also enter the Ras signaling pathway to activate MAPK [49]. The activated MAPK translocates to the nucleus to upregulate pro-neurogenic transcription factors, thereby promoting neural differentiation [49]. Hence the results above, would clearly implicate mechanotransduction in the enhancement of neural differentiation by electrical charge. Additionally, the PI3K/Akt/mTOR signaling pathway can be triggered by ErbB-2/4, which had been demonstrated to be closely associated with the maturation of neural stem cells and the development of neural tubes by several studies [50,51].

4. Conclusions

In summary, this study characterized the dose-response effects of surface charge mediated by the $BaTiO_3$/P(VDF-TrFE) nanocomposite membranes on neural differentiation of SHED, and preliminarily explored the possible underlying molecular mechanisms involved. Both earlier and later neurogenic differentiation of SHED appear to be dose-dependently enhanced by surface charge, as manifested by changes in cell morphology, including increased cell spreading area, cell elongation and more prominent neurite outgrowths. Further investigations of the underlying molecular mechanisms revealed that surface charge stimulates opening of calcium channels on the cell membrane. The resulting increase in intracellular calcium concentration might activate pro-neurogenic signaling pathways, such as the FAK-ERK mechanosensing pathway and ErbB signaling pathway, as well as induce remodeling of actin cytoskeleton. Hence, this study confirms the dose-responsive effects of biomaterial surface charge-induced SHED neural differentiation and provides preliminary insights into the underlying molecular mechanisms and signaling pathways involved.

Ethics approval and consent to participate

Stem cells from human exfoliated deciduous teeth (SHED) were provided by ORAL STEM CELL BANK run by Beijing Tason Biotech Co., Ltd. (http://www.kqgxbk.com). This study does not involve animal experiments and clinical patient recruitment.

CRediT authorship contribution statement

Xiaochan Li: Investigation, Formal analysis, Methodology, Software, Validation, Writing – original draft. **Boon Chin Heng:** Methodology, Funding acquisition, Writing – review & editing. **Yunyang Bai:** Investigation, Methodology, Validation. **Qianqian Wang:** Methodology, Validation. **Min Gao:** Investigation, Methodology. **Ying He:** Investigation, Validation. **Xinwen Zhang:** Conceptualization, Project administration, Writing – review & editing. **Xuliang Deng:** Conceptualization, Funding acquisition, Project administration, Writing – review & editing. **Xuehui Zhang:** Conceptualization, Funding acquisition, Supervision, Project administration, Writing – review & editing.

Declaration of interest statement

The authors declare that they have no competing interests.

Acknowledgments

This work was supported by the National Key Research and Development Program of China (2021YFB3800800, 2021YFC2400400), the National Natural Science Foundation of China (Nos. 82022016, 81991505, 51973004, 52103312), the Beijing Municipal Natural Science Foundation (7222226) and Peking University Medicine Fund (PKU2020LCXQ009).

Appendix A. Supplementary data

Supplementary data to this article can be found online at https://doi.org/10.1016/j.bioactmat.2022.05.007.

References

[1] D.O. Dias, H. Kim, D. Holl, B. Werne Solnestam, J. Lundeberg, M. Carlén, et al., Reducing pericyte-derived scarring promotes recovery after spinal cord injury, Cell 173 (1) (2018) 153–165, https://doi.org/10.1016/j.cell.2018.02.004, e122. e-pub ahead of print 2018/03/06.
[2] S.G. Varadarajan, J.L. Hunyara, N.R. Hamilton, A.L. Kolodkin, A.D. Huberman, Central nervous system regeneration, Cell 185 (1) (2022) 77–94, https://doi.org/10.1016/j.cell.2021.10.029, e-pub ahead of print 2022/01/08.
[3] I.J. Fox, G.Q. Daley, S.A. Goldman, J. Huard, T.J. Kamp, M. Trucco, Stem cell therapy. Use of differentiated pluripotent stem cells as replacement therapy for treating disease, Science 345 (6199) (2014) 1247391, https://doi.org/10.1126/science.1247391, e-pub ahead of print 2014/08/26.
[4] V. Tabar, L. Studer, Pluripotent stem cells in regenerative medicine: challenges and recent progress, Nat. Rev. Genet. 15 (2) (2014) 82–92, https://doi.org/10.1038/nrg3563, e-pub ahead of print 2014/01/18.
[5] N.C. Spitzer, Electrical activity in early neuronal development, Nature 444 (7120) (2006) 707–712, https://doi.org/10.1038/nature05300, e-pub ahead of print 2006/12/08.
[6] J. Wang, H. Wang, X. Mo, H. Wang, Reduced graphene oxide-encapsulated microfiber patterns enable controllable formation of neuronal-like networks, Adv. Mater. 32 (40) (2020), e2004555, https://doi.org/10.1002/adma.202004555 e-pub ahead of print 2020/09/03.

[7] R. Zhu, Z. Sun, C. Li, S. Ramakrishna, K. Chiu, L. He, Electrical stimulation affects neural stem cell fate and function in vitro, Exp. Neurol. 319 (2019) 112963, https://doi.org/10.1016/j.expneurol.2019.112963, e-pub ahead of print 2019/05/28.

[8] L. He, Z. Sun, J. Li, R. Zhu, B. Niu, K.L. Tam, et al., Electrical stimulation at nanoscale topography boosts neural stem cell neurogenesis through the enhancement of autophagy signaling, Biomaterials 268 (2021) 120585, https://doi.org/10.1016/j.biomaterials.2020.120585, e-pub ahead of print 2020/12/12.

[9] W. Guo, X. Zhang, X. Yu, S. Wang, J. Qiu, W. Tang, et al., Self-powered electrical stimulation for enhancing neural differentiation of mesenchymal stem cells on graphene-poly(3,4-ethylenedioxythiophene) hybrid microfibers, ACS Nano 10 (5) (2016) 5086–5095, https://doi.org/10.1021/acsnano.6b00200, e-pub ahead of print 2016/05/05.

[10] Z. Liu, M. Cai, X. Zhang, X. Yu, S. Wang, X. Wan, et al., Cell-traction-triggered on-demand electrical stimulation for neuron-like differentiation, Adv. Mater. 33 (51) (2021), e2106317, https://doi.org/10.1002/adma.202106317 e-pub ahead of print 2021/10/17.

[11] J. Kwon, J.S. Lee, J. Lee, J. Na, J. Sung, H.J. Lee, et al., Vertical nanowire electrode array for enhanced neurogenesis of human neural stem cells via intracellular electrical stimulation, Nano Lett. 21 (14) (2021) 6343–6351, https://doi.org/10.1021/acs.nanolett.0c04635, e-pub ahead of print 2021/05/18.

[12] R. Zhang, S. Han, L. Liang, Y. Chen, B. Sun, N. Liang, et al., Ultrasonic-driven electrical signal-iron ion synergistic stimulation based on piezotronics induced neural differentiation of mesenchymal stem cells on FeOOH/PVDF nanofibrous hybrid membrane, Nano Energy 87 (2021) 106192, https://doi.org/10.1016/j.nanoen.2021.106192.

[13] S. Manipatruni, D.E. Nikonov, C.C. Lin, T.A. Gosavi, H. Liu, B. Prasad, et al., Scalable energy-efficient magnetoelectric spin-orbit logic, Nature 565 (7737) (2019) 35–42, https://doi.org/10.1038/s41586-018-0770-2, e-pub ahead of print 2018/12/05.

[14] Y. Bai, X. Dai, Y. Yin, J. Wang, X. Sun, W. Liang, et al., Biomimetic piezoelectric nanocomposite membranes synergistically enhance osteogenesis of deproteinized bovine bone grafts, Int. J. Nanomed. 14 (2019) 3015–3026, https://doi.org/10.2147/ijn.S197824, e-pub ahead of print 2019/05/24.

[15] C. Zhang, W. Liu, C. Cao, F. Zhang, Q. Tang, S. Ma, et al., Modulating surface potential by controlling the β phase content in poly(vinylidene fluoridetrifluoroethylene) membranes enhances bone regeneration, Adv, Healthc, Mater, 7 (11) (2018), e1701466, https://doi.org/10.1002/adhm.201701466 e-pub ahead of print 2018/04/21.

[16] X. Zhang, C. Zhang, Y. Lin, P. Hu, Y. Shen, K. Wang, et al., Nanocomposite membranes enhance bone regeneration through restoring physiological electric microenvironment, ACS Nano 10 (8) (2016) 7279–7286, https://doi.org/10.1021/acsnano.6b02247, e-pub ahead of print 2016/07/09.

[17] B. Tang, B. Zhang, J. Zhuang, Q. Wang, L. Dong, K. Cheng, et al., Surface potential-governed cellular osteogenic differentiation on ferroelectric polyvinylidene fluoride trifluoroethylene films, Acta Biomater. 74 (2018) 291–301, https://doi.org/10.1016/j.actbio.2018.04.051, e-pub ahead of print 2018/05/08.

[18]a G.T. Huang, S. Gronthos, S. Shi, Mesenchymal stem cells derived from dental tissues vs. those from other sources: their biology and role in regenerative medicine, J. Dent. Res. 88 (9) (2009 Sep) 792–806.

[19]a K. Sakai, A. Yamamoto, K. Matsubara, S. Nakamura, M. Naruse, M. Yamagata, K. Sakamoto, R. Tauchi, N. Wakao, S. Imagama, H. Hibi, K. Kadomatsu, N. Ishiguro, M. Ueda, Human dental pulp-derived stem cells promote locomotor recovery after complete transection of the rat spinal cord by multiple neuro-regenerative mechanisms, J. Clin. Invest. 122 (1) (2012 Jan) 80–90.

[20]a R. Kunimatsu, K. Nakajima, T. Awada, Y. Tsuka, T. Abe, K. Ando, T. Hiraki, A. Kimura, K. Tanimoto, Comparative characterization of stem cells from human exfoliated deciduous teeth, dental pulp, and bone marrow-derived mesenchymal stem cells, Biochem. Biophys. Res. Commun. 501 (1) (2018 Jun 18) 193–198.

[21]a T. Yamaza, A. Kentaro, C. Chen, Y. Liu, Y. Shi, S. Gronthos, S. Wang, S. Shi, Immunomodulatory properties of stem cells from human exfoliated deciduous teeth, Stem Cell Res. Ther. 1 (1) (2010 Mar 15) 5.

[18]b X. Shi, J. Mao, Y. Liu, Pulp stem cells derived from human permanent and deciduous teeth: biological characteristics and therapeutic applications, Stem Cell. Transl. Med. 9 (4) (2020) 445–464, https://doi.org/10.1002/sctm.19-0398, e-pub ahead of print 2020/01/17.

[19]b B.C. Heng, S. Jiang, B. Yi, T. Gong, L.W. Lim, C. Zhang, Small molecules enhance neurogenic differentiation of dental-derived adult stem cells, Arch. Oral Biol. 102 (2019) 26–38, https://doi.org/10.1016/j.archoralbio.2019.03.024, e-pub ahead of print 2019/04/08.

[20]b Z. Zhu, G. Rui, R. Li, H. He, L. Zhu, Enhancing electrostrictive actuation via strong electrostatic repulsion among field-induced nanodomains in a relaxor ferroelectric poly(vinylidene fluoride-co-trifluoroethylene-co-chlorotrifluoroethylene) random terpolymer, ACS Appl. Mater. Interfaces 13 (35) (2021) 42063–42073, https://doi.org/10.1021/acsami.1c12745, e-pub ahead of print 2021/08/27.

[21]b N. Soin, D. Boyer, K. Prashanthi, S. Sharma, A.A. Narasimulu, J. Luo, et al., Exclusive self-aligned β-phase PVDF films with abnormal piezoelectric coefficient prepared via phase inversion, Chem. Commun. 51 (39) (2015) 8257–8260, https://doi.org/10.1039/c5cc01688f, e-pub ahead of print 2015/04/16.

[22] P. Sharma, H.T. Cline, Visual activity regulates neural progenitor cells in developing xenopus CNS through musashi1, Neuron 68 (3) (2010) 442–455, https://doi.org/10.1016/j.neuron.2010.09.028, e-pub ahead of print 2010/11/03.

[23]a M. Forouzanfar, L. Lachinani, K. Dormiani, M.H. Nasr-Esfahani, A.O. Gure, K. Ghaedi, Intracellular functions of RNA-binding protein, Musashi1, in stem and cancer cells, Stem Cell Res. Ther. 11 (1) (2020 May 24) 193.

[23]b E. Telek, A. Kengyel, B. Bugyi, Myosin XVI in the nervous system, Cells 9 (8) (2020), https://doi.org/10.3390/cells9081903 e-pub ahead of print 2020/08/23.

[24] A. Pocaterra, G. Santinon, P. Romani, I. Brian, A. Dimitracopoulos, A. Ghisleni, et al., F-actin dynamics regulates mammalian organ growth and cell fate maintenance, J. Hepatol. 71 (1) (2019) 130–142, https://doi.org/10.1016/j.jhep.2019.02.022, e-pub ahead of print 2019/03/18.

[25] R. Wu, A. Li, B. Sun, J.G. Sun, J. Zhang, T. Zhang, et al., A novel m(6)A reader Prrc2a controls oligodendroglial specification and myelination, Cell Res. 29 (1) (2019) 23–41, https://doi.org/10.1038/s41422-018-0113-8, e-pub ahead of print 2018/12/06.

[26] D. Sun, X.P. Xie, X. Zhang, Z. Wang, S.F. Sait, S.V. Iyer, et al., Stem-like cells drive NF1-associated MPNST functional heterogeneity and tumor progression, Cell Stem Cell 28 (8) (2021) 1397–1410, https://doi.org/10.1016/j.stem.2021.04.029, e1394. e-pub ahead of print 2021/05/20.

[27] K. Kuwako, K. Kakumoto, T. Imai, M. Igarashi, T. Hamakubo, S. Sakakibara, et al., Neural RNA-binding protein Musashi1 controls midline crossing of precerebellar neurons through posttranscriptional regulation of Robo3/Rig-1 expression, Neuron 67 (3) (2010) 407–421, https://doi.org/10.1016/j.neuron.2010.07.005, e-pub ahead of print 2010/08/11.

[28] Z.R. Lybrand, S. Goswami, J. Zhu, V. Jarzabek, N. Merlock, M. Aktar, et al., A critical period of neuronal activity results in aberrant neurogenesis rewiring hippocampal circuitry in a mouse model of epilepsy, Nat. Commun. 12 (1) (2021) 1423, https://doi.org/10.1038/s41467-021-21649-8, e-pub ahead of print 2021/03/05.

[29] R. Gómez, L.E. Maglio, A.J. Gonzalez-Hernandez, B. Rivero-Pérez, D. Bartolomé-Martín, T. Giraldez, NMDA receptor-BK channel coupling regulates synaptic plasticity in the barrel cortex, Proc. Natl. Acad. Sci. U. S. A. 118 (35) (2021), https://doi.org/10.1073/pnas.2107026118 e-pub ahead of print 2021/08/29.

[30] D.J. Simon, D.M. Belsky, M.E. Bowen, Ohn Cyj, M.K. O'Rourke, R. Shen, et al., An anterograde pathway for sensory axon degeneration gated by a cytoplasmic action of the transcriptional regulator P53, Dev. Cell 56 (7) (2021) 976–984, https://doi.org/10.1016/j.devcel.2021.03.011, e973. e-pub ahead of print 2021/04/07.

[31] A. Tchoghandjian, C. Jennewein, I. Eckhardt, S. Momma, D. Figarella-Branger, S. Fulda, Smac mimetic promotes glioblastoma cancer stem-like cell differentiation by activating NF-κB, Cell Death Differ. 21 (5) (2014) 735–747, https://doi.org/10.1038/cdd.2013.200, e-pub ahead of print 2014/02/04.

[32]a F. Sgrò, F.T. Bianchi, M. Falcone, G. Pallavicini, M. Gai, A.M. Chiotto, G.E. Berto, E. Turco, Y.J. Chang, W.B. Huttner, F. Di Cunto, Tissue-specific control of midbody microtubule stability by Citron kinase through modulation of TUBB3 phosphorylation, Cell Death Differ. 23 (5) (2016 May) 801–813.

[32]b S.C. Hung, H. Cheng, C.Y. Pan, M.J. Tsai, L.S. Kao, H.L. Ma, In vitro differentiation of size-sieved stem cells into electrically active neural cells, Stem Cell. 20 (6) (2002) 522–529, https://doi.org/10.1634/stemcells.20-6-522, e-pub ahead of print 2002/11/29.

[33] R. Ikeda, M.S. Kurokawa, S. Chiba, H. Yoshikawa, M. Ide, M. Tadokoro, et al., Transplantation of neural cells derived from retinoic acid-treated cynomolgus monkey embryonic stem cells successfully improved motor function of hemiplegic mice with experimental brain injury, Neurobiol. Dis. 20 (1) (2005) 38–48, https://doi.org/10.1016/j.nbd.2005.01.031, e-pub ahead of print 2005/09/03.

[34] Y. Song, D. Li, O. Farrelly, L. Miles, F. Li, S.E. Kim, et al., The mechanosensitive ion channel piezo inhibits axon regeneration, Neuron 102 (2) (2019) 373–389, https://doi.org/10.1016/j.neuron.2019.01.050, e376. e-pub ahead of print 2019/03/02.

[35] W.Z. Zeng, K.L. Marshall, S. Min, I. Daou, M.W. Chapleau, F.M. Abboud, et al., PIEZOs mediate neuronal sensing of blood pressure and the baroreceptor reflex, Science 362 (6413) (2018) 464–467, https://doi.org/10.1126/science.aau6324, e-pub ahead of print 2018/10/27.

[36] D.W. Zhou, M.A. Fernández-Yagüe, E.N. Holland, A.F. García, N.S. Castro, E. B. O'Neill, et al., Force-FAK signaling coupling at individual focal adhesions coordinates mechanosensing and microtissue repair, Nat. Commun. 12 (1) (2021) 2359, https://doi.org/10.1038/s41467-021-22602-5, e-pub ahead of print 2021/04/23.

[37] K. Zhang, Z. Jia, B. Yang, Q. Feng, X. Xu, W. Yuan, et al., Adaptable hydrogels mediate cofactor-assisted activation of biomarker-responsive drug delivery via positive feedback for enhanced tissue regeneration, Adv. Sci. 5 (12) (2018) 1800875, https://doi.org/10.1002/advs.201800875, e-pub ahead of print 2018/12/26.

[38] S.Z. Chen, L.F. Ning, X. Xu, W.Y. Jiang, C. Xing, W.P. Jia, et al., The miR-181d-regulated metalloproteinase Adamts1 enzymatically impairs adipogenesis via ECM remodeling, Cell Death Differ. 23 (11) (2016) 1778–1791, https://doi.org/10.1038/cdd.2016.66, e-pub ahead of print 2016/10/19.

[39] N. Strohmeyer, M. Bharadwaj, M. Costell, R. Fässler, D.J. Müller, Fibronectin-bound α5β1 integrins sense load and signal to reinforce adhesion in less than a second, Nat. Mater. 16 (12) (2017) 1262–1270, https://doi.org/10.1038/nmat5023, e-pub ahead of print 2017/11/09.

[40] L.B. Case, M. De Pasquale, L. Henry, M.K. Rosen, Synergistic phase separation of two pathways promotes integrin clustering and nascent adhesion formation, Elife 11 (2022), https://doi.org/10.7554/eLife.72588 e-pub ahead of print 2022/01/21.

[41] L. Gauthier, S. Corgnac, M. Boutet, G. Gros, P. Validire, G. Bismuth, et al., Paxillin binding to the cytoplasmic domain of CD103 promotes cell adhesion and effector functions for CD8(+) resident memory T cells in tumors, Cancer Res. 77 (24) (2017) 7072–7082, https://doi.org/10.1158/0008-5472.Can-17-1487, e-pub ahead of print 2017/10/13.

[42] C.G. Gahmberg, M. Grönholm, How integrin phosphorylations regulate cell adhesion and signaling, Trends Biochem. Sci. (2021), https://doi.org/10.1016/j.tibs.2021.11.003 e-pub ahead of print 2021/12/08.

[43] Y. Guo, F. Mei, Y. Huang, S. Ma, Y. Wei, X. Zhang, et al., Matrix stiffness modulates tip cell formation through the p-PXN-Rac1-YAP signaling axis, Bioact. Mater. 7 (2022) 364–376, https://doi.org/10.1016/j.bioactmat.2021.05.033, e-pub ahead of print 2021/09/02.

[44] B. Laplace-Builhé, A. Barthelaix, S. Assou, C. Bohaud, M. Pratlong, D. Severac, et al., NRG1/ErbB signalling controls the dialogue between macrophages and neural crest-derived cells during zebrafish fin regeneration, Nat. Commun. 12 (1) (2021) 6336, https://doi.org/10.1038/s41467-021-26422-5, e-pub ahead of print 2021/11/05.

[45] P. Banerjee, G.Y. Xiao, X. Tan, V.J. Zheng, L. Shi, M.N.B. Rabassedas, et al., The EMT activator ZEB1 accelerates endosomal trafficking to establish a polarity axis in lung adenocarcinoma cells, Nat. Commun. 12 (1) (2021) 6354, https://doi.org/10.1038/s41467-021-26677-y, e-pub ahead of print 2021/11/05.

[46] X. Li, L.H. Klausen, W. Zhang, Z. Jahed, C.T. Tsai, T.L. Li, et al., Nanoscale surface topography reduces focal adhesions and cell stiffness by enhancing integrin endocytosis, Nano Lett. 21 (19) (2021) 8518–8526, https://doi.org/10.1021/acs.nanolett.1c01934, e-pub ahead of print 2021/08/05.

[47] V.K. Lim Lam, J.Y. Hin Wong, S.Y. Chew, B.P. Chan, Rac1-GTPase regulates compression-induced actin protrusions (CAPs) of mesenchymal stem cells in 3D collagen micro-tissues, Biomaterials 274 (2021) 120829, https://doi.org/10.1016/j.biomaterials.2021.120829, e-pub ahead of print 2021/05/03.

[48] Y.W. Chiu, L.Y. Liou, P.T. Chen, C.M. Huang, F.J. Luo, Y.K. Hsu, T.C. Yuan, Tyrosine 397 phosphorylation is critical for FAK-promoted Rac1 activation and invasive properties in oral squamous cell carcinoma cells, Lab. Invest. 96 (3) (2016 Mar) 296–306.

[49] K. Frebel, S. Wiese, Signalling molecules essential for neuronal survival and differentiation, Biochem. Soc. Trans. 34 (Pt 6) (2006 Dec) 1287–1290.

[50] L. Wang, K. Zhou, Z. Fu, D. Yu, H. Huang, X. Zang, et al., Brain development and akt signaling: the crossroads of signaling pathway and neurodevelopmental diseases, J. Mol. Neurosci. 61 (3) (2017) 379–384, https://doi.org/10.1007/s12031-016-0872-y, e-pub ahead of print 2016/12/28.

[51] C. Tehranian, L. Fankhauser, P.N. Harter, C.D.H. Ratcliffe, P.S. Zeiner, J. M. Messmer, et al., The PI3K/Akt/mTOR pathway as a preventive target in melanoma brain metastasis, Neuro Oncol. 24 (2) (2022) 213–225, https://doi.org/10.1093/neuonc/noab159, e-pub ahead of print 2021/07/04.